Spring 2018

# Improved Thermal Stability of Cesium-Doped Perovskite Films With PMMA for Solar Cell Application

Christine M. Gausin
*Old Dominion University*

# IMPROVED THERMAL STABILITY OF CESIUM-DOPED PEROVSKITE FILMS WITH PMMA FOR SOLAR CELL APPLICATION

by

Christine M. Gausin
B.S. May 2018, Old Dominion University

A Thesis Submitted to the Faculty of
Old Dominion University in Partial Fulfillment of the
Requirements for the Degree of

MASTER OF SCIENCE

ELECTRICAL AND COMPUTER ENGINEERING

OLD DOMINION UNIVERSITY
May 2018

Approved by:

_____
Gon Namkoong (Director)

_____
Christopher Bailey (Member)

_____
Helmut Baumgart (Member)

## ABSTRACT

IMPROVED THERMAL STABILITY OF CESIUM-DOPED PEROVSKITE FILMS WITH PMMA FOR SOLAR CELL APPLICATION

Christine M. Gausin
Old Dominion University, 2018
Director: Dr. Gon Namkoong

Perovskite solar cells (PSCs) have the potential to replace the traditional silicon solar cells for commercialization applications. Perovskites offer a lower cost to fabrication, superb efficiencies, high absorption coefficients, longer carrier lifetime and diffusion lengths. Despite their improved efficiency, perovskites suffer from several degradations relating to the material's organic-inorganic composition upon exposure to different environmental conditions. In general, the main causes of degradation of perovskite films are due to exposure to moisture, oxygen, air, light, and temperature. Several efforts have been made to stabilize perovskites including encapsulation, doping of cations, and alterations to the perovskite structure. In this work, we study the effect of PMMA and cesium (Cs) on the thermal stability of perovskite solar cells.

Due to the organic composition of perovskite solar cells (PSCs), the material has high sensitivity to moisture, air, oxygen, light and heat. Upon exposure to these sensitive factors, perovskite films undergo degradation very quickly, resulting in a reduced efficiency and unstable cell. To better improve the material's stability, we study the effect of adding a PMMA layer on top of the $MAPbI_3$ samples, induced at 85°C to study whether PMMA has a major effect not only in protecting the layer from degradation factors, but also on its thermal stability. XRD measurements confirmed that samples without the PMMA layer quickly showed signs of degradation after 72 hours of heating with the peak formation of $PbI_2$. $MAPbI_3$ samples with the PMMA were able to withstand heating up to 1000 hours with minor sign of the $PbI_2$ peak. SEM images confirmed the

degradation of the samples without PMMA as indicated by pinholes forming along the grain boundaries and grain of the samples, while samples with the PMMA showed very little signs of degradation.

We further studied the thermal stability of perovskite solar cells by heating the samples at a more aggressive temperature (120°C) and study the effects of cesium on the precursor solution. Due to $MAPbI_3$'s susceptibility to degradation at higher temperatures, cesium was added to the precursor solution at different concentrations (x = 5, 9 and 20%) to form the $Cs_xMA_{1-x}PbI_3$ formula. XRD data showed that after 72 hours of thermal treatment, samples with the cesium content withheld the perovskite samples from complete degradation. Data for the $MAPbI_3$ reference sample showed complete degradation after the 72 hours, as indicated by the very intense peak formation of $PbI_2$.

I dedicate this thesis to my very supportive mother, Imelda Gausin, for teaching me to never give up and to always strive for success regardless of the obstacles and struggles I face.

## ACKNOWLEDGMENTS

This work was funded and supported by the National Science Foundation's SoLar Engineering Academic Program (SoLEAP, contract number 1355678). I would have not been able to pursue my graduate degree without the help of this funding. I would like to acknowledge three faculty from Old Dominion University's (ODU) Department of Electrical and Computer Engineering (ECE), who have all been influential in my interest in the photovoltaic (PV) area, and my decision to go beyond my bachelor's degree.

My first hands-on experience with PV research was under Dr. Sylvain Marsillac's Microelectronics Device Fabrication Lab, ECE 387 course. This lab, which followed the course of Microelectronic Materials and Processes (also taught by Dr. Marsillac), sparked my interest in the PV field. His enthusiasm in this field along with his willingness to make sure that his students understood his lectures encouraged me to become really interested in this area and later register for the fabrication lab course. In ECE 387, we were given the opportunity to implement what we had learned in the pre-requisite course by experiencing the hands-on work involved in fabrication of a semiconductor device. I always enjoy hands-on work labs because it gives me the opportunity to apply what I had already learned, and I also gain the experience first-hand. Because of this course, I started gearing my courses towards solar and renewable energy.

Following the lab course, I was given the opportunity to be granted the SoLEAP scholarship as directed by Dr. Gon Namkoong. Dr. Namkoong became my advisor under the scholarship. He gave me the opportunity to further my knowledge of solar cells by providing me with resources to study for simulating current-voltage characteristic of perovskite cells, along with being a project to build a temperature-dependent stage. Dr. Namkoong's research is towards the inorganic-organic solar cells, which allowed me to expand my knowledge of the various aspects

and areas of solar cells that I didn't know about. Since I have been working under Dr. Namkoong's, I joined his project for the senior design course. I gained more hands-on experience during this course as I was given the opportunity to travel to the Applied Research Center (ARC) at Jefferson Lab in Newport News. I worked with Dr. Namkoong's PhD candidates during my experience at the lab, and I was taught about the functionalities of the perovskite cell and its characteristic. Furthermore, I learned to fabricate perovskite solar cells and characterize the samples through current-voltage (JV) measurements. Upon nearing my completion of my bachelor's degree, Dr. Namkoong convinced me to pursue a M.S. degree under his instruction.

Pursuing a M.S. degree was a big step forward from my undergraduate's degree. I was having doubts on whether to pursue the accelerated program as I had the opportunity to have a full-time job already available for me upon completion of my undergraduate's degree. Dr. Christopher Bailey helped clear any doubts and questions I had about pursuing a higher education degree. Given his undergrad background in Mechanical Engineering, he gave me insight into his journey during his undergrad and his sudden spark of interest in the PV field. Dr. Bailey did not hesitate to talk to me about my doubts, and he volunteered to answer any questions I had regarding an advanced degree. He also volunteered to let me shadow under one of his students, Sean Babcock. Dr. Bailey became my unofficial mentor and my go-to professor for any advice in the PV field and pursuing of an advanced degree. Without Dr. Bailey's compassion and willingness to help guide students in the right path and give them the opportunity to have that experience to be in that field without fully committing, I would have probably doubted pursuing an advanced degree for a longer time.

I further acknowledge my fellow graduate research colleagues Abdullah Al Mamun, Tanzila Ava, and Loi Nguyen for guiding me in my pursuant of my degree, as well as continuously

encouraging me to learn more and answering any questions I had regarding the perovskite solar cell structure and characteristics. I also want to acknowledge Dr. Wei Cao for being so patient and allowing me to book the characterization labs for several hours and even days for my research. I want to thank all others who continuously supported me and believed in my academic endeavors, providing advice and guidance throughout the challenges I faced.

# NOMENCLATURE

| | |
|---|---|
| *GB* | Grain boundary |
| *PCE* | Power conversion efficiency |
| *PSC* | Perovskite solar cell |
| *PV* | Photovoltaic |
| *SEM* | Scanning electron microscope |
| *XRD* | X-Ray diffraction |

# TABLE OF CONTENTS

Page

# LIST OF FIGURES

# CHAPTER 1

# INTRODUCTION

## 1.1 Renewable Energy

Renewable energy has been the source of power for many ancient civilizations for several thousands of years including human powered treadmills, wind energy for sail ships, and even solar energy to ignite fires [1]. Ancient civilization had no access to any technologies that would convert non-renewable energy sources like fossil fuels to be their main primary source of energy due to lack of technological advancement, and even lack of use. Fossil fuels, a form of non-renewable energy, did not become so apparent and popular until the Industrial Revolution that took place in the $18^{th}$ century. The Industrial Revolution marked an era of technological advancement and the need for sources of energy, from which petroleum, coal and natural gas became the ideal and most abundant sources at that time. Fossil fuels were abundant sources at that time and were formed from organic material that had been in Earth over the course of millions of years. Fossil fuels have fueled and become the main energy source for many economic and technological advancements of the Industrial Era. Fossil fuels, however, have the disadvantage of forming emissions of carbon dioxide ($CO_2$), which has been the leading cause for global warming, extreme weather conditions and decline in the ozone layer [2]. $CO_2$ emission has since doubled across the world since 1975. Thus, there has been great interest in finding alternative sources of "clean energy" that would not harm the environment and be sufficient to support the demand of energy globally [3].

The International Energy Agency (IEA) foresees an increase of demand in energy globally by 30% between 2017 and 2040 [4]. Because of this, a major shift in the industry has led to harvesting renewable energy sources, which are forms of energy that can easily be replenished

naturally. According to the IEA, rapid development in renewable energy could increase power generation by 40% in efforts led by China and India [4]. Some of these energy sources include biomass, geothermal heat, sunlight, water, and wind. Among these energy sources, solar energy has captured a wide array of interests in research and application. Solar energy is a form of renewable energy that relies on the sun's rays for electricity and/or thermal energy. Because of the abundance of solar energy, a great deal of research and development has been focused on developing cutting-edge technology that will replace the dependence on fossil fuels. Photovoltaics (PV) is one of the leading field in this development.

### 1.2 Photovoltaic (PV)

PV devices were first discovered by a team of scientists at Bell Telephone, which realized that silicon had the ability to create an electric charge upon exposure to sunlight. Photovoltaic devices, most commonly known as solar cells, convert the energy coming from the sun directly into electricity. The sun is comprised of photons, which are particles of solar energy that can be absorbed by semiconductor materials that form a PV device. Photons from the sun have varying energy corresponding to the different wavelengths of the solar spectrum. As photons strike a PV cell, several cases may happen: a photon is reflected off the cell, it passes through the cell completely, or it is absorbed by the semiconductor material [5]. Only absorbed photons can convert to generate electricity. Thus, a great deal of research and development (R&D) funds have been dedicated to investigating the types of semiconductor materials that can absorb a wide range of wavelengths to convert the most photons into energy. According to the National Renewable Energy Laboratory's (NREL) efficiency chart below, the power conversion efficiency (PCE) of solar cells currently ranges from 10.6% to 46%.

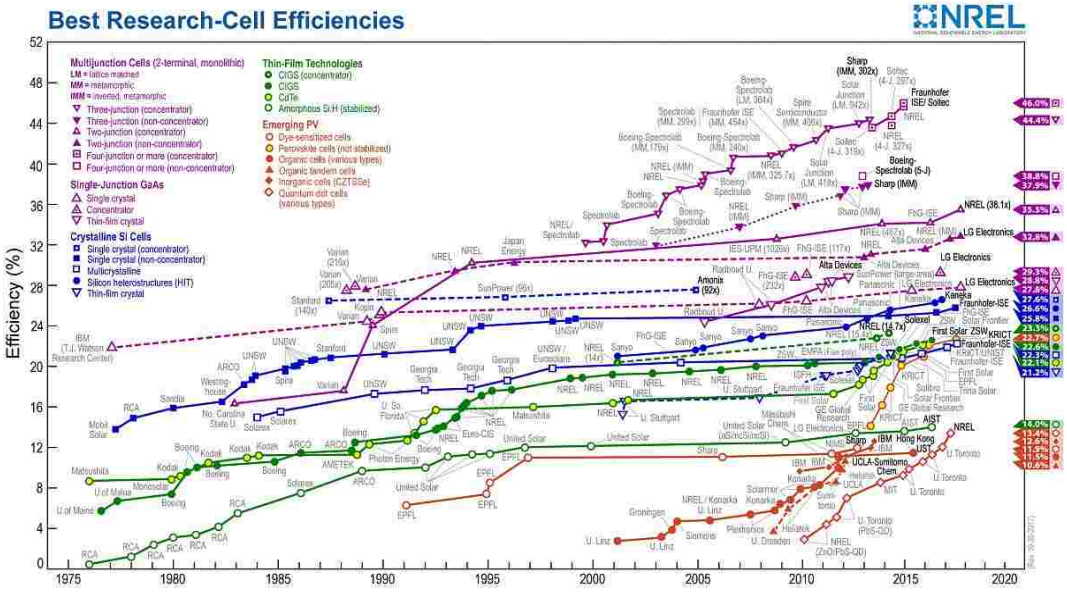


**Figure 1**. NREL's Efficiency Chart ("Best Research-Cell Efficiencies" is reprinted with permission by the National Renewable Energy Laboratory, Accessed April 23, 2018)

As can be seen in Figure 1, PV devices range from multijunction cells to even thin-film technologies. Traditional solar cells are generally fabricated from silicon and prove to be the most efficient and are found commercially available in the market. Thin-film solar cells followed the first-generation solar cells and were termed "second-generation" solar cells due to the reduction of thickness, along with their given flexibility, while still retaining most of the efficiency of traditional silicon cells. Third-generation solar cells use other types of materials other than silicon, including organic materials or polymers. Currently, emerging third-generation solar cells are gaining the interest of many researchers as they can replace the currently used silicon solar cells by lowering the cost of fabrication and outputting comparable and even higher efficiencies.

### 1.2.1 Perovskite Solar Cells (PSCs)

Perovskite solar cells (PSCs) are one of promising new generation solar cells that incorporate a mixed organic-inorganic material to harvest the energy from the sun. Organic-inorganic halide perovskites have emerged to be one of the leading PV technologies with increasing efficiencies in less than a decade, low fabrication cost, high carrier mobility, and large absorption characteristics [6] – [9]. Perovskites have the crystal $ABX_3$ structure, where A forms the organic cation, B is the metal cation, and X is the halogen anion [9]. Many organic cations that have been used have typically been methylammonium (MA), or formamidinium (FA), while lead (Pb) and tin (Sn) have been commonly used for the divalent metal ion. The common halide ions that have been used in the perovskite structure has been iodine (I), bromine (Br) and chlorine (Cl).

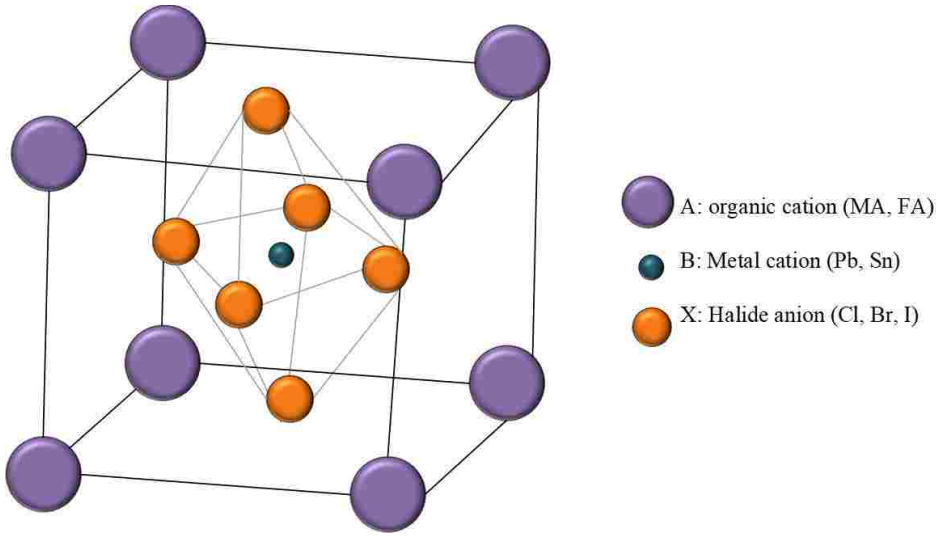


**Figure 2**. Chemical structure of perovskite in the $ABX_3$ form

Given such free-form structure, the composition of a perovskite structure can easily be modified to maximize its performance, whether it is to increase efficiency or improve its stability. The most commonly used perovskite structure is the $MAPbI_3$, from which the methylammonium compound, also known as $CH_3NH_3$, has shown promising efficiencies and stability [10], [11]. In

2009, the recorded efficiency for perovskite solar cells were marked at 3.8% and in just less than a decade, the PCE of the cell has jumped to 22.7% proving that the material is a promising candidate for future PV technology application [12].

### 1.3 Structural Stability

The $ABX_3$ perovskite form does not always result in a perfect perovskite phase as the precursor material have the flexibility to arrange themselves into various crystalline or amorphous phases which causes several issues when implemented as a PV technology [13]. The structure of perovskites can undergo multiple thermal annealing during film deposition, which does not always yield a stable phase at normal operating temperatures. There have been studies as to which A, B cations, and X anions should occupy the structure to best produce a stable perovskite phase. In its cubic phase, the lead halide octahedra's size is determined by the size and electronegativity of the B and X ions and it also further determines the volume from which the A cation can occupy. Much of the orientation of the crystal structure relies heavily on the A cation size, such that if this size is large or even relatively small, the octahedral form needs to tilt or distort to accommodate the difference. The small distortions in the crystal structure relate to the orthorhombic and tetragonal phase of the perovskite. These two phases share similar optoelectronic properties such as small shifts in band gap, carrier lifetime, and electron/hole mobilities. If the mismatch between the lead halide octahedral size and the A cation size is too large to accommodate, the compound will not be in a perovskite phase. Furthermore, understanding the tolerance factor of the lead halide octahedra's distortion and tilting provides information on the possible phases the material could exist and indicate whether the material can form a crystal structure. The cubic phase's tolerance

factor is known to be t = 1, while the deviation between tetragonal or orthorhombic ranges from $0.7 < t < 0.9$ [13].

There have been other numerous studies attempting to understand the advantages and disadvantages of the distinct phases of perovskite at varying phases. The three structural phases as mentioned before for the $MAPbI_3$ perovskite include a cubic phase (>56°C), tetragonal phase (-113 to +56°C) and orthorhombic phase (<56°C) [14]. The orthorhombic phase is known to have fully ordered MA cations, while tetragonal phase has partially ordered MA cations and the cubic phase has fully disordered MA cations. Phase transition among the three phases has been studied previously to understand what the impact of phase transitions on the optical, thermal, dielectric, and PV characteristic of a perovskite sample [14].

The common applied perovskite form, $MAPbI_3$, has been studied to be in its perovskite phase at room temperature, with a tetragonal distortion. When the temperature is reduced, the material then deviates to its orthorhombic phase. As the temperature is increased, the material transitions into its cubic phase. Because $MAPbI_3$ can exist at two distinct phases between relevant temperatures of 0 to +100°C, this material has low susceptibly to structural degradation in its lifetime. However, this does not prevent $MAPbI_3$ to be prone to outside factor degradation including air, moisture, water, oxygen, UV-light and heat

### 1.3.1 Instability of Perovskites

Although this organic-inorganic material proves to be a promising candidate for the future of photovoltaics technologies, perovskites suffer from degradation due to its organic material composition. Multiple degradation factors have been identified correlating to the $MAPbI_3$ structure including temperature, moisture, oxygen, electric-field, UV-light and heat [15], [16]. The

following chemical reaction was proposed to explain the thermal degradation of perovskite solar cells [17]:

$$\mathbf{CH_3NH_3PbI_3} \overset{\mathbf{H_2O}}{\longleftrightarrow} \mathbf{CH_3NH_3I\,(aq) + PbI_2(s)} \quad (1)$$

$$\mathbf{CH_3NH_3I\,(aq)} \leftrightarrow \mathbf{CH_3NH_2(aq) + HI\,(aq)} \quad (2)$$

$$\mathbf{4HI\,(aq) + O_2} \leftrightarrow \mathbf{2I_2(s) + 2H_2O} \quad (3)$$

$$\mathbf{2HI\,(aq)} \overset{\mathbf{hv}}{\leftrightarrow} \mathbf{H_2} \uparrow \mathbf{+I_2(s)} \quad (4)$$

When the chemical mixture of perovskite ($CH_3NH_3PbI_3$) is exposed to water, it undergoes hydrolysis. This reaction results in the formation of lead iodide ($PbI_2$) and $CH_3NH_3I$ solutions, which are the some of the primary signs of degradation of the perovskite sample. Decomposition of the $CH_3NH_3I$ solution into the methylamine ($CH_3NH_2$) and hydroiodic acid (HI) solutions results in the formation of $I_2$ and $H_2O$ from the reaction formed by HI with oxygen molecules [17]. Further studies have also shown that when perovskite is exposed to sunlight, it corrodes the $CH_3NH_3PbI_3$ to form $PbI_2$ [18].

Because of the organic material of the perovskite solution, it makes it easier for these degradation factors to seep into the grains and grain boundaries and cause areas to be defective and therefore, reduce the performance of the device. Therefore, several studies have been conducted to better aid the device in its major challenge: thermal stability. Upon exposure to thermal heating, $CH_3NH_3PbI_3$ goes under chemical mass loss and degradation as listed in the equations below [19].

$$\mathbf{CH_3NH_3PbI_3} \overset{\mathbf{\Delta}}{\leftrightarrow} \mathbf{NH_3 + CH_3I + PbI_2} \quad (5)$$

$$\mathbf{CH_3NH_3I} \overset{\mathbf{\Delta}}{\leftrightarrow} \mathbf{NH_3 + CH_3I} \quad (6)$$

$$\mathbf{CH_3NH_3^+\,(g) + I^-(g)} \rightarrow \mathbf{CH_3NH_2(aq) + HI\,(aq)} \quad (7)$$

$$\mathbf{CH_3NH_3I \overset{\Delta}{\leftrightarrow} NH_3 + CH_3I} \quad (8)$$

Thermal degradation of $MAPbI_3$ is surface initiated, and is a layer by layer reaction, and therefore the decomposition of the methylammonium ions ($CH_3NH_3^+$) is assisted by iodide through the process called reverse Menshutkin reaction. This reaction is a process of simultaneously breaking the C-N bond, which typically is common for quaternary ammonium salts. However, in the decomposition of methylammonium, ammonia is produced rather than trimethylamine $(CH_3)_3N$ [19]. The further degradation of perovskites is initiated at the weak Pb-I-Pb bonds along the (001) plane, where $PbI_2$ prefers a relaxed trigonal structure. The remaining $CH_3NH_3^+$ and $I^-$ ions in $\mathbf{CH3NH_3I \overset{\Delta}{\leftrightarrow} NH_3 + CH_3I}$ ( **6** create a reaction that releases the $CH_3NH_2$ and HI gas from the sample. Due to the thermal decomposition of $MAPbI_3$ into $PbI_2$ under a surface reaction, degradation is kinetically preferred along the surface, exposing the first layer and decomposing it until the next layer degrades and the process goes on and on until the entire perovskite material is completely degraded [19].

MA forming the A cation in the crystal structure of the $ABX_3$ form of the perovskite suffers from its own instability such as heat. There have been several researchers involved in attempting to replace the MA cation with other cations including the larger FA cation, and or simply replacing the organic cation with an inorganic cesium (Cs) for a more thermally stable solar cell. However, research in this field is still ongoing on determining which combination, or which cation can withstand thermal stability while still outputting high efficiencies.

### 1.4 Motivation

Commercially available photovoltaic technologies are mostly comprised of silicon-based devices. Silicon is an abundant element source, and thus makes this material a probable option for

commercialization. However, silicon-based solar cells have reached a saturation in efficiency only improving at about 2.7% in the last ten years [20], [21]. Although the pricing for silicon-based materials have decreased in the last seven years, the cost of production has continuously increased [22]. Silicon-based solar cells must undergo multiple stages of fabrication, which increases the cost for production as more machines and materials are needed to fabricate one solar cell wafer. The need to reduce the cost of commercialization while still producing highly efficient and stable cells is becoming more and more apparent today. According to the NREL efficiency chart, the top-performing multi-crystalline silicon cell is currently at 22.3%, while the more expensive single-crystal silicon cell is currently rated at 25.8%. Third-generation PVs have emerged to be possible candidates for replacement of the more traditional silicon solar cells. Perovskite solar cell (PSC), one of the emerging PVs of today has shown major improvements, especially in efficiency in just less than ten years. NREL's efficiency chart records the current efficiency for perovskite to sit at 22.7%, which is slightly higher than the multi-crystalline silicon cell. Furthermore, the fabrication of PSCs does not require expensive equipment, nor do they take a long time. Perovskite solar cells have been studied to produce the highest efficiencies using sol-gel method (process of settling nano-sized particles from a colloidal solution deposited onto a substrate by spin-coating or other methods), while other methods have shown promising results such as hot-casting technique. However, much improvement must be made before this inorganic-organic material can be largely commercialized.

The work discussed in this paper explores some of the top priorities in improving the perovskite solar cell including its crystal structure, film quality, and thermal stability. Perovskite solar cells are prone to degradation upon exposure to moisture, light, heat, water, and oxygen. Under these environmental conditions, the material easily degrades as these defects travel through

the pinholes, and gaps in the perovskite crystal grain causing internal instability. With the presence of moisture, perovskite solar cells undergo degradation in a matter of hours. Furthermore, perovskite solutions decompose to $PbI_2$ upon exposure with moisture. With the presence of moisture and water, the photo conversion efficiency and optical properties of the perovskite material quickly deteriorates resulting in a lower stability, and poor device performance. The polymer poly(methyl methacrylate) (PMMA) layer has been studied to help passivate any defect on perovskite solar cells and aid in preventing moisture from degrading the crystal grain of the film [23], [24]. PMMA has been proven to delocalize any captured carries at the deep trap areas forming on the perovskite surface, as well as modify the surface of the structure to passivate defected areas [25]. With the delocalization of trapped carriers and passivation of surface defects, PMMA aids in improving device performance by increasing $J_{sc}, V_{oc}$ $and$ $FF$ [26]. By improving the film quality of the crystal (fabricating films with larger crystal grains, and smaller grain boundaries), the film quality of the perovskite can easily improve on having fewer defects that degrade the crystal grains. Moreover, crystal growth and film quality are improved with the addition of PMMA, as it is known to improve crystal growth and increase crystal size [26]. PMMA has been fabricated in a complete perovskite solar cell with efficiencies exceeding 18% [23], [24]. Another key area that remains a challenge preventing perovskites from future commercialization is its thermal stability. Solar cells that must meet certification for industrial manufacturing must meet the operating temperature between -40 to +85℃ as well as have a lifespan of 20 years or more [27]. Given such wide and elevated temperature range for commercialization, the study of thermal stability of perovskites proves to be one of the leading challenges that must be addressed first. $MAPbI_3$ perovskite solar cells suffer from thermal instability as mentioned in Section 1.3.1. $MAPbI_3$ films suffer from mechanical stress and degradation due to poor thermal conductivity

[28], [29]. To resolve this issue, several studies have mentioned replacing the MA cation in the conventionally used perovskite with FA and such replacement has proven a more stable perovskite under higher temperatures. However, FA-based perovskites are still prone to degradation to oxygen due to oxidation and are more sensitive to moisture in comparison to MA-based perovskites [26]. Other studies have completely replaced A in the $ABX_3$ form with cesium (Cs) to produce highly stable perovskites at temperatures reaching 300℃. However, Cs-based perovskites have non-ideal band gaps (>1.7 eV), which produces lower PCEs in comparison to other perovskite-based materials [26]. The work described here will study the thermal degradation of perovskite solar cells ($MAPbI_3$) and show improvements upon addition of PMMA by thermally heating the sample at 85C for 1000 hours period. Furthermore, cesium is doped into the mixture to form $Cs_xMA_{1-x}PbI_3$ and show how doping this cation improves the stability of perovskites at higher temperatures.

**1.5 Methodology**

To achieve a stable perovskite solar cell, PMMA was added on top of the precursor solution upon a hot casting technique. $MAPbI_3$ samples with and without PMMA were induced to a thermal treatment at 85°C to study the known thermal degradation of perovskites, along with confirming the improved stability upon addition of PMMA. To further improve the thermal stability of perovskites, MA-based perovskite samples were fabricated with different concentration of cesium (Cs). MA-based perovskites have shown promising efficiencies but prove to be less stable upon exposure to different temperatures. To investigate the effects of cesium on the MA-based perovskite samples, different concentrations of cesium were doped: x = 5%, x = 9%, x = 20% to form the following chemical formula $Cs_xMA_{1-x}PbI_3$ using the hot-casting technique for sample

preparations. The $Cs_xMA_{1-x}PbI_3$ samples were heated at 85°C and a more thermally aggressive temperature, 120℃, to determine how cesium will aid in the thermal stability of the samples. The captured SEM images allow to identify areas of defects, with formation of pinholes along the grain boundaries, as well as confirm the duration of stability for the samples as confirmed by the XRD data.

# CHAPTER 2

# EXPERIMENTAL

In this thesis, the $MAPbI_3$ and $Cs_xMA_{1-x}PbI_3$ samples were prepared via hot casting technique (where the temperature of the substrate and the temperature of the solution must retain to be at a certain temperature before spin-coating). Due to the ease of fabrication of perovskite solar cells, only a spin-coating machine and a hot plate was required for fabrication. However, due to the samples sensitivity to moisture and oxygen, the samples were stored inside a nitrogen glovebox. To characterize the $MAPbI_3$ and $Cs_xMA_{1-x}PbI_3$ samples, different characterization techniques were needed including x-ray diffraction (XRD) and scanning electron microscopy (SEM).

## 2.1 Solution Preparation

Fluorine doped tin oxide coated (FTO) glasses were used as the substrate for the precursor solution deposition. These FTO substrates were cleaned in a five-step sonication process using mucosal, deionized (DI) water, methanol, acetone and 2-propanol (IPA) for a 10-minute duration per each cleaning step. The FTO substrates were then dried with nitrogen and heated for 15 minutes at 120℃ on a hot plate to remove any remaining traces of the solvents used. The Cs-doped perovskite ($Cs_xMA_{1-x}PbI_3$) precursor solution was prepared by incorporating the hot casting technique with the three concentrations of cesium iodide (CsI) (x = 5%, 9%, and 20%). The $MAPbI_3$ precursor was prepared by dissolving equimolar ratios of lead iodide ($PbI_2$, Sigma-Aldrich, 99%) and methylamine hydrochloride (MAI, Sigma-Aldrich) in N,N-dimethylformamide (DMF, Sigma-Aldrich, anhydrous, 99.8%) to a concentration of 11 wt%. The cesium-doping

involved preparing three types of solution with the respected concentration of cesium and were heated on a hot plate for 18 hours at 70℃ with magnetic stirring in a nitrogen ($N_2$) filled glove box. The temperature for the solution and the FTO substrate must retain to be at 180°C and at 70°C, respectively upon spin-coating at 4000rpm. Some samples prepared were coated with PMMA by spin-coating the polymethyl-methacrylate (PMMA, Mw ~ 120,000) in chlorobenzene (10mg/ml) at 4000rpm for 10 seconds.

## 2.2 Characterization

In this work, characterization techniques involving the x-ray diffraction (XRD) and scanning electron microscopy (SEM) were used to determine degradation of the samples (if any at all) with morphology, crystal structure, absorption, and optical quality of the $MAPbI_3$ and $Cs_xMA_{1-x}PbI_3$ samples. The following subsections will provide a full detailed explanation of each material characterization techniques used.

### 2.2.1 X-ray Diffraction (XRD)

This work utilized the Rigaku Miniflex II benchtop XRD instrument along with the integrated X-ray powder diffraction software, PDXL provided by Rigaku to verify the crystal information of the samples measured. The data collected were ranged from 5 – 70° at the $2\theta$ range with an acquisition rate of 5°/min with a step size of 0.02°. The $2\theta$ range was used to cover the different preferred orientation of the perovskite phase at 14.08°, 28.44°, 31.85°, 40.58°, 43.19° assigned to the (110), (220), (310), (224) and (330) planes. Minor peaks exist at the following planes indicating the high phase purity of the perovskite films at 19.92°, 23.54°, 24.52°, 39.94°, 50.22° and 52.54° corresponding to the (200), (211), (312), (404) and (226) planes [26] – [28]. $PbI_2$ peaks would start becoming more apparent if the samples started degrading at the following

plane (001) corresponding to 12.6° [27] – [33]. For investigation of the thermal stability of $Cs_xMA_{1-x}PbI_3$ solar cells, only the major known peaks were closely observed: 12.6° (001), 14.08° (110), and 28.44° (220).

X-ray diffraction incorporates the constructive interference technique, where two waves with the same wavelength align and interact to form a resulting wave with much bigger amplitude than the original waves. X-ray diffraction not only employs constructive interference to gather information about the sample, it is one of the most important non-destructive techniques when it comes to material characterization. X-ray diffraction provides critical information about a sample's structural information and crystalline phase. X-ray wavelengths were identified to be the main light source for the diffractometer upon discovery that the three-dimensional (3D) diffraction resembled that of the crystal lattice spacing on a crystalline substance [34]. An X-ray diffractometer typically consists of an x-ray light source, a sample holder, and x-ray detector. The generation of x-rays initiate upon heating of the filament of the cathode x-ray tube to produce electrons, which are accelerated towards a given target. The target material produces specific wavelengths unique to its own, and some known target materials include copper (Cu), iron (Fe), molybdenum (Mo) and chromium (Cr). Most XRD equipment use copper as the base target material for characterization [35], [36].

Due to the accelerated bombardment of electrons onto the target material, several electrons on the core shell of the Cu atoms are ejected, producing vacancies that are quickly filled by electrons dropping from higher levels. Therefore, an X-ray spectrum is emitted during the process of ejection and filling of vacancies. The X-ray spectra produce information on the transition of electrons between the atomic energy levels of the K-shells (n = 1). K$\alpha$ spectras contain information about the transition from the n = 2 and n = 1 levels of filling the vacant electrons, while K$\beta$

provides the energy transition from n = 3 to n = 1. The production of the K-shell spectrum is typically determined by the target material used with its specific wavelength corresponding to the shell transition for vacancy filling. Using the CuK$\alpha$ light source ($\lambda = 1.5418$ Å), only the K$\alpha$ radiation is filtered into the monochromatic x-rays and is directed onto the sample material for bombardment. The incident x-ray beams that bombard the sample produces diffracted x-rays that are detected and recorded by the x-ray detector. Figure 3 depicts the relationship between the incident x-rays, the d-spacing of the atoms, and the diffracted x-rays. This relationship, known as Bragg's Law, plays a critical role in X-ray diffraction. Bragg's Law states that the diffracted x-rays that reflect from the sample contain diffracted peaks at a range of various $2\theta$ angles from which the samples were measured.

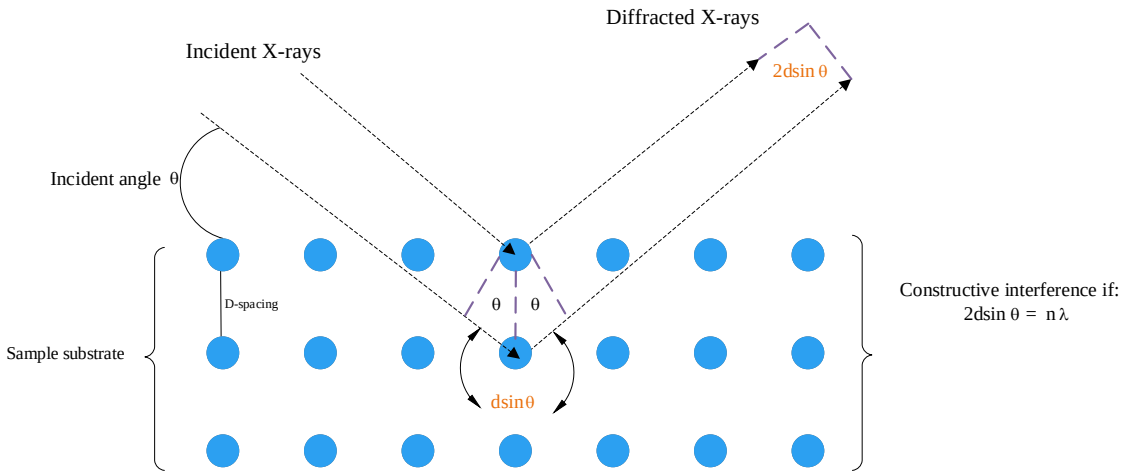


**Figure 3**.Bragg's Law of x-ray diffraction.

Bragg's Law provides a relationship between the d-spacing ($d$) of the atoms to the angle of incidence ($\theta$), the wavelength of the x-ray source ($\lambda$) and the order of reflection ($n$) defined as

$$\boldsymbol{n\lambda = 2dsin\theta}. \qquad (9)$$

The relationship provided by Bragg's Law allows for the extraction of information relating to the identification of an unknown sample, crystal geometry, and lattice information. The lattice constant *a* of the sample, for example, can be extracted given the known crystal's geometry (known as the Miller indices hkl) *d* as described below

$$\boldsymbol{d} = \frac{\boldsymbol{a}}{\sqrt{\boldsymbol{h^2+k^2+l^2}}}. \qquad (10)$$

The diffracted beams are measured by the detector when Bragg's law is satisfied upon constructive interference. The diffractometer counts the pulses per unit time, which are directly proportional to the intensity of the diffracted beams of the x-rays, and a plotted image of the peaks are outputted by the software. Several databases exist to confirm which peaks correlate to specific materials such as the International Centre for Diffraction Data (ICDD) and provide for quick identification of the material. Given the raw file produced by the diffractometer software, additional provided by the equipment such as that of Rigaku's PDXL software provides a way to extract more information from the given XRD data. A number of kinds of information such as the crystal size, stress-and-strain, and crystallinity of the sample can be provided easily when the XRD data is loaded into the PDXL software.

2.2.2 Scanning Electron Microscope (SEM)

The images captured in this report were collected by JEOL JSM-6400LV. Images were captured at an accelerating voltage of 15kV with different magnification conditions as indicated in the image scale bar. Due to the organic material of the samples, a thin conductive layer of gold (Au) was coated on the surface of the $Cs_xMA_{1-x}PbI_3$ samples using a Hummer V Sputter Coater. The samples were measured at different magnifications ranging from $10\mu m$ to $1\mu m$ to give a better overall image of the grain size and grain boundaries (GB) as well as a zoomed in view to give a better view of the possible degradation occurring on the grains and GBs.

# CHAPTER 3

# THERMAL DEGRADATION OF PEROVSKITE FILMS AND CS-DOPED PEROVSKITE FILMS

In this work, samples of $MAPbI_3$ and $Cs_xMA_{1-x}PbI_3$ were prepared as mentioned in Section 2.1 without PMMA. The reference sample ($MAPbI_3$) was thermally treated at both 85°C and 120°C to observe the length of stability of perovskite solar cells without PMMA. $Cs_xMA_{1-x}PbI_3$ was also induced to thermal treatment at 85°C to observe the effect of Cs-doped perovskite solar cells on the thermal stability of the solar cell. Both the reference and $Cs_xMA_{1-x}PbI_3$ samples without PMMA did not sustain more than 72 hours of heating at 85°C before showing signs of degradation as indicated by the $PbI_2$ peak. The reference sample, $MAPbI_3$ was further heated at 120°C to observe the stability of MA-based perovskites at higher temperatures. This section will provide a detailed discussion and complete analysis of the data resulting from SEM, and XRD.

## 3.1 $MAPbI_3$ without PMMA heated at 85°C

This section will discuss the $MAPbI_3$ sample fabricated without PMMA. The XRD peaks exist at 14.08°, and 28.44° corresponding to the perovskite (110), and (220). The $PbI_2$ peak started becoming prominent at 12.6°, corresponding to the (001) plane. It can be noted that the perovskite peak at 14.08° decreases over time as the sample is heated. Furthermore, signs of degradation started becoming apparent at the 72 hours reading as indicated by the formation of the $PbI_2$ peak. As the sample were heated past 72 hours, the $PbI_2$ peak increased at an alarming rate showing complete degradation of the sample after the 528 hours heating.

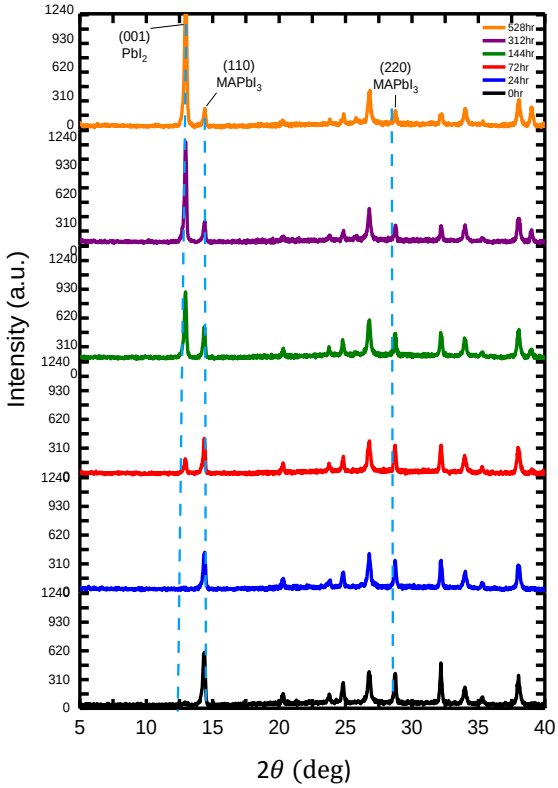


**Figure 4.** XRD data for $MAPbI_3$ without PMMA sample heated at 85°C for 528 hours.

The integrated intensity of the XRD peaks were plotted to further show the inverse relationship between the perovskite and $PbI_2$ peak at 14.08° (110) and 12.6° (001) respectively. As the samples were thermally treated over the period of experimentation, the integrated intensity for the perovskite peak corresponding to the (110) plane decreased and reached a saturation point around the 312 hours reading. The integrated intensity for the $PbI_2$ peak linearly increased over time, clearly concluding that the sample is degraded. To further investigate the effect of degradation of the perovskite films, the crystal size was calculated using the Scherrer equation:

$$\boldsymbol{L} = \frac{\mathbf{K\lambda}}{\boldsymbol{\beta}\mathbf{cos\theta}} \qquad (11)$$

where $L$ is the average crystal size, $\lambda$ is the wavelength of the X-ray source ($\mathrm{CuK}\alpha = 1.5418\,\text{Å}$ or $0.15418\,nm$), and $\beta$ is the full width at half maximum (FWHM). Upon thermal treatment, the crystal size for the $PbI_2$ peak increased while the crystal size for the $MAPbI_3$ peak deceased. This confirms the degradation effect as observed in the integrated intensity plot, the XRD data and the SEM images.

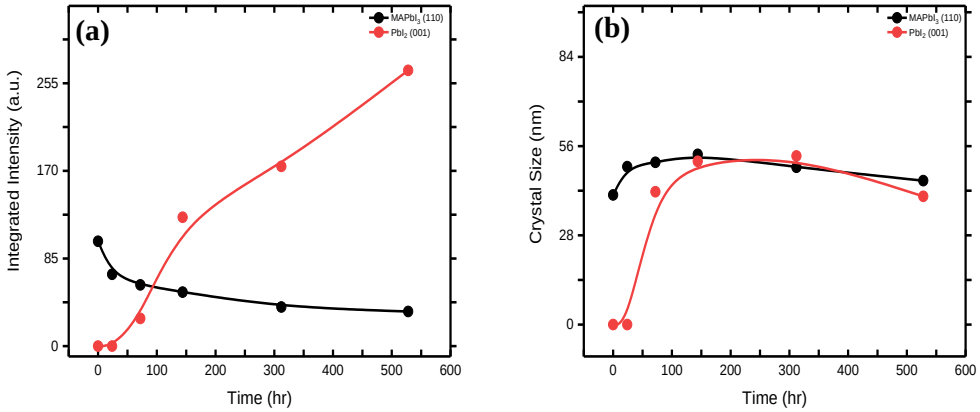


**Figure 5.** $MAPbI_3$ without PMMA's (a) XRD integrated intensity and (b) crystal size for (110) and (001) planes.

The data is further confirmed by the captured SEM images below Figure 6(a) shows poor morphological structure with a rough surface and grainy structure. The initial image at 0 hour, as indicated by Figure 6(a) shows no signs of degradation in comparison to the 72 hour heating in **Figure 6**(b). In Figure 6(b), signs of degradation started becoming more prominent along the grain boundaries (GBs). The crystal grain surface of the $MAPbI_3$ sample started showing signs of roughness and formation of pinholes (dark spots) around the edge of the grains. As the samples are induced to the thermal treatment over time, the pinholes started moving towards the center of the grains, as can be seen in Figure 6(c). The $1\mu m$ magnification of the SEM image shows that the

pinholes after the 72 hours heating is not as deep in comparison to the pinholes forming at the 528 hours reading. This means that the longer the samples are being heated, the deeper the pinholes form, making it easier for heat to degrade the perovskite layer by layer.

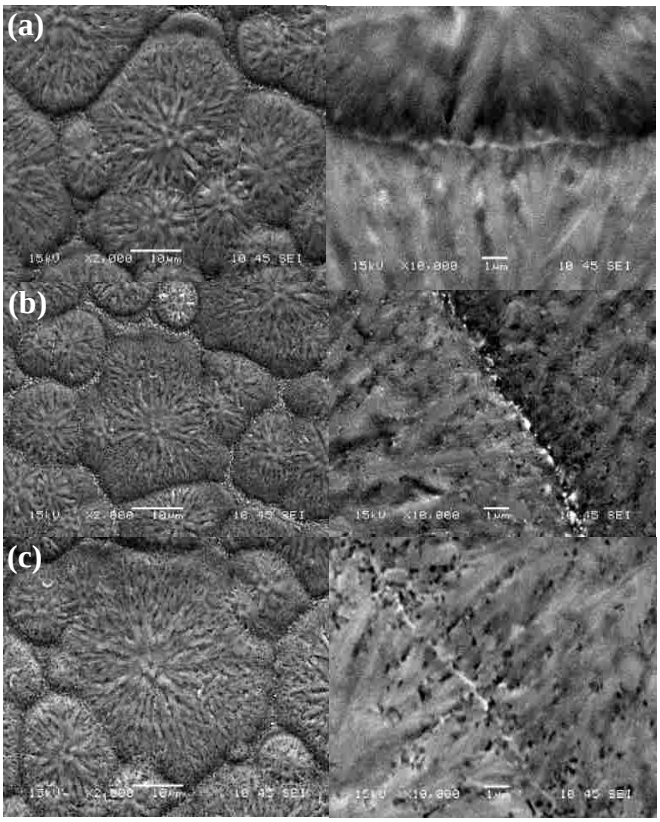


**Figure 6.** SEM images for $MAPbI_3$ without PMMA taken at (a) 0hr, (b) 72hrs and (c) 528hrs.

### 3.2 $Cs_xMA_{1-x}PbI_3$ without PMMA heated at 85℃

This section will discuss the $Cs_xMA_{1-x}PbI_3$ samples without PMMA heated at 85℃. Samples were prepared as detailed win Section 2.1. The XRD peaks exist at 14.08°, and 28.44° corresponding to the perovskite planes at (110), and (220) and the $PbI_2$ peak at 12.6°,

corresponding to the (001) plane. Note that the perovskite peak at 14.08° decreases with increasing cesium content, as indicated by the XRD data in

Figure 7(a). The SEM images in

Figure 7(b) – (d) correspond to the samples x = 20%, x = 9% and x = 5%. An interesting feature to note is that the "root-like" structure located towards the center of the grains of the perovskite surface is much bigger with lower cesium content.

Comparing

Figure 7(b) and

Figure 7(d) shows that the grain surface of the x = 5% sample is grainier and rougher in comparison to the smooth surface of the x = 20% sample. Furthermore, the x = 9% sample exhibits the largest grain size in comparison to the rest of the samples.

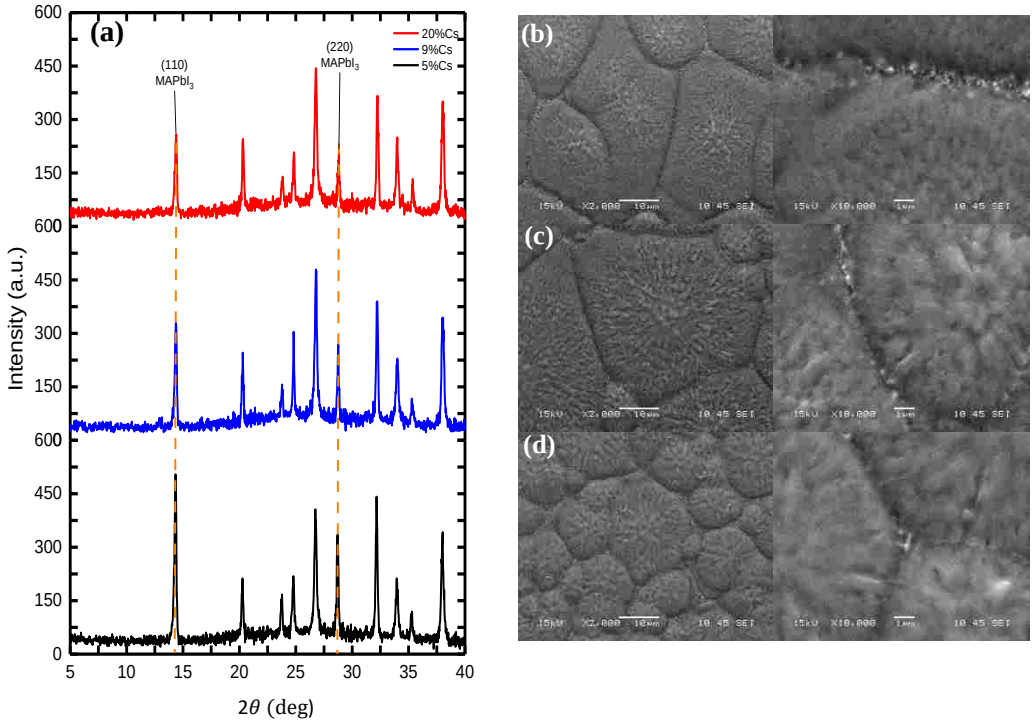


**Figure 7.** (a) XRD data and SEM images for (b) 20%, (c) 9%, and (d) 5% Cesium-doped perovskite samples before thermal treatment.

After 72 hours of thermal treatment, the $Cs_xMA_{1-x}PbI_3$ samples started showing signs of degradation upon appearance of the $PbI_2$ peak at 12.6° and formation of pinholes along the GBs. The x = 20% sample exhibits the highest degradation rate in comparison to the x = 5% and x = 9% sample, as can be seen in the XRD data in **Error! Reference source not found.**(a). This could be due to lower amount of $MAPbI_3$ solution. The x = 5% sample maintains the highest $MAPbI_3$ peak, and the lowest $PbI_2$ peak at the (110) and (001) planes, indicating superb stability even with the smaller grains along the surface. The SEM images shows the formation of pinholes (dark spots) around the GBs andgrains. Furthermore, the "root-like" structure as mentioned before is expanding almost covering the entire grain of the surface of the films. The smaller grains of the x = 5% Cs

sample exhibit more pinholes all around, while the larger sized grains of the sample, only exhibit pinholes along the edge of the crystal grain as indicated by **Error! Reference source not found.**(d). This confirms the theory that a better film quality is needed to prevent further

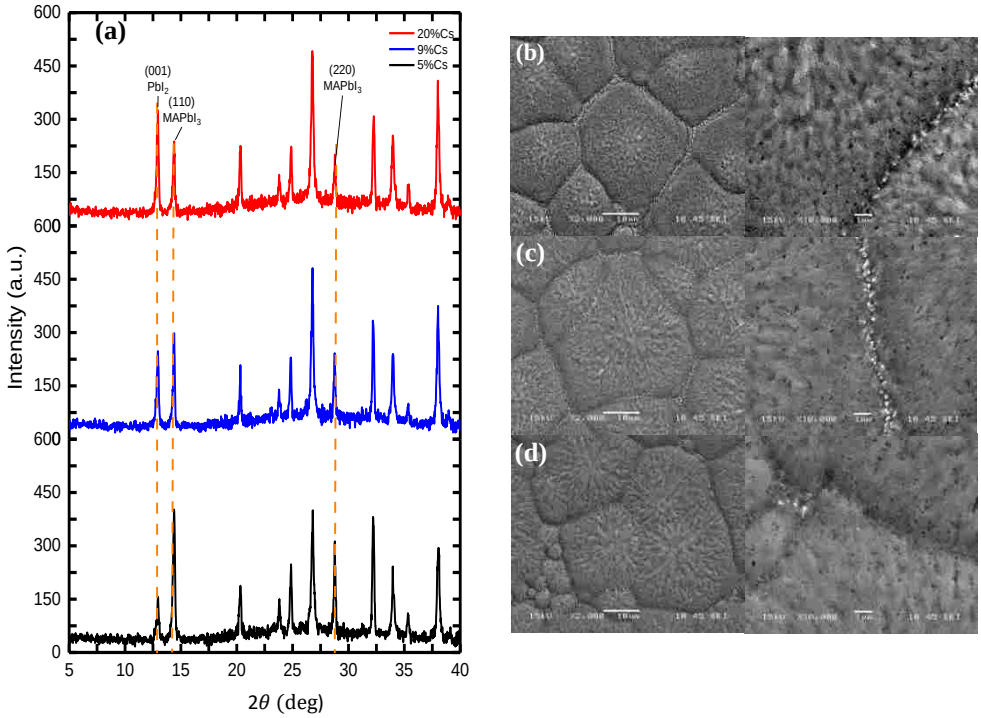


degradation of the crystals of perovskite films. The pinhole on the x = 20% sample is scattered not only along the grain boundaries but are reaching the center of the grain surface. The pinholes are also much darker, which could indicate that these pinholes are deeper which could confirm the reason why the degradation rate of this sample is much faster than the rest of the other samples. Initially the surface of the x = 20% sample was smoother, but upon thermal treatment, the surface started becoming grainier and rough as indicated by the $1\mu m$ magnification image.

**Figure 8.** (a) XRD data and SEM images for (b) 20%, (c) 9%, and (d) 5% Cesium-doped perovskite samples after 72 hours of thermal treatment.

The $Cs_xMA_{1-x}PbI_3$ completely degraded after 528 hours of thermal treatment. The $PbI_2$ peak at 12.6° showed supreme dominance over the perovskite peak at 14.08°. Figure 9(a) shows complete degradation for the x = 20% sample with a very low peak still located at 14.08°

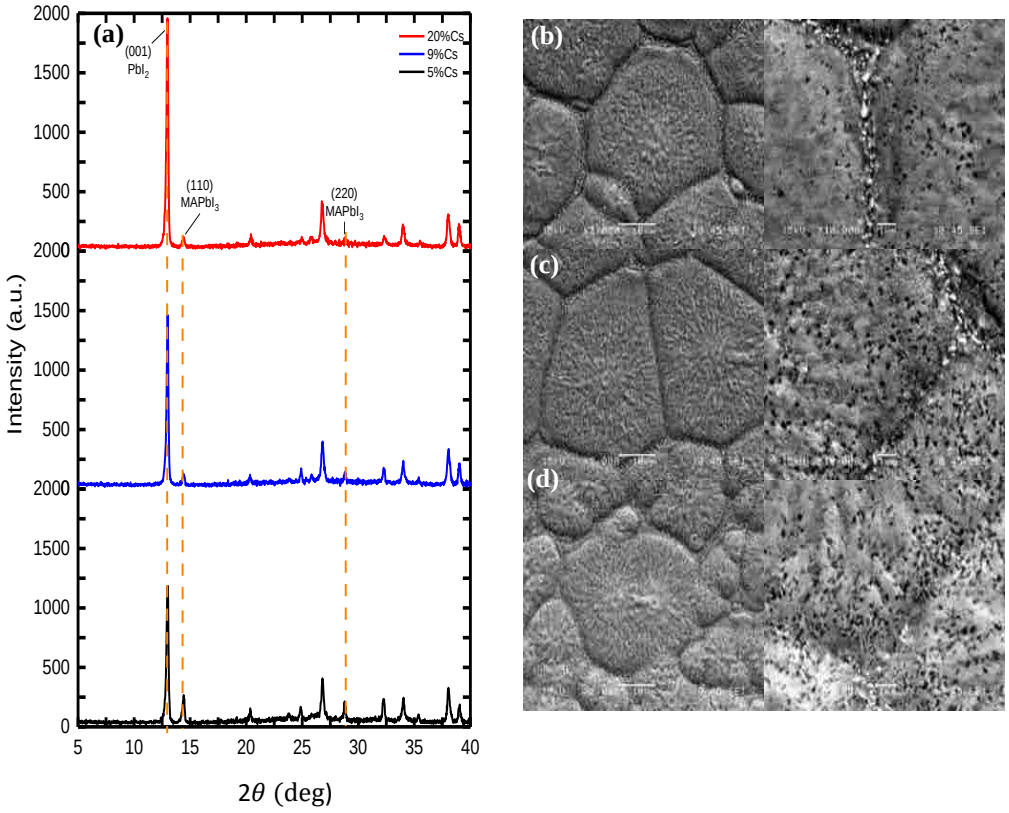


corresponding to the perovskite (110) plane peak. The x = 5% sample maintained a still visible height for the perovskite peak even after 528 hours of thermal treatment. The SEM images show the morphological degradation of the samples with complete pinhole coverage along the grains and GBs.

**Figure 9**. (a) XRD data and SEM images for (b) 20%, (c) 9%, and (d) 5% Cesium-doped perovskite samples after 528 hours of thermal treatment.

### 3.3 $MAPbI_3$ without PMMA heated at 120℃

This section will discuss the $MAPbI_3$ sample fabricated without PMMA and induced to thermal heating at 120℃. The XRD peaks exist at 14.08°, and 28.44° corresponding to the perovskite (110), and (220). The $PbI_2$ peak started becoming prominent at 12.6°, corresponding to the (001) plane. **Error! Reference source not found.** represents the XRD data and SEM images captured for the duration of the experiment. Prior to thermal heating at the aggressive temperature of 120°C, no signs of degradation were present on the XRD data nor the SEM captured images. The surface of the $MAPbI_3$ sample shows the "root-like" structure present towards the center of the grain, but is not as rough or as prominent in comparison to the same surface formation in the $MAPbI_3$ sample heated at 85°C in Figure 6(a). The XRD data in **Error! Reference source not found.**(a) indicate that the sample suffered thermal instability upon thermal treatment and prior to the 24 hours reading given the relatively low perovskite peak existing at 14.08°. At the 72 hours reading, the perovskite peak is no longer present and the $PbI_2$ peak at 12.6° is now five times the height of the original perovskite peak. The captured SEM images present some interesting data with the "root-like" structure almost not being present, and several dark spots forming all over the grain structure at the higher magnification image. Furthermore, the $1\mu m$ magnification shows "cracked-like" structures along the grain boundaries of the sample with the high presence of pinholes (dark pots). Upon recording of the images at the 72 hours reading, the sample is completely covered in pinholes. The closer magnification shows very deep pinholes suggesting that the sample has decomposed the last layer of the perovskite and the sample has degraded completely. From the $1\mu m$ magnification, it is clear to note that the grain boundary can no longer be differentiated from the grains, as the pinholes covered the sample completely. This suggests

that MA-based perovskite solar cells are prone to degradation and instability upon thermal treatment at higher temperatures (in this case, 120°C).

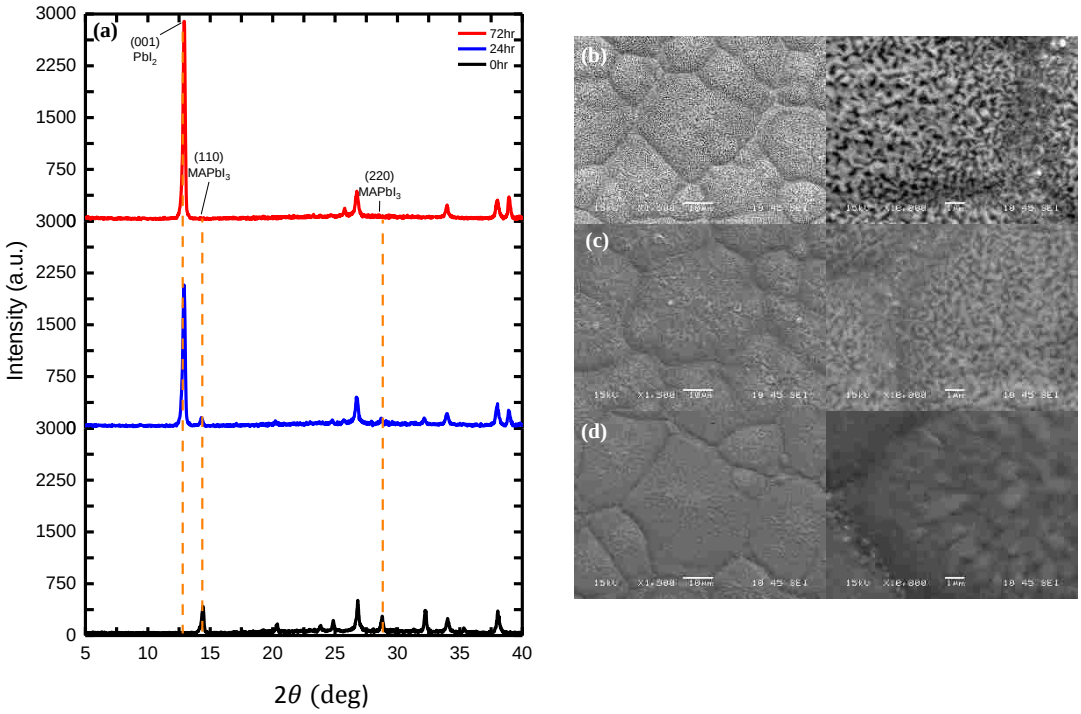


**Figure 10.** (a) XRD data and SEM images captured at (b) 72hr, (c) 24hr, and (d) 0hr upon thermal heating of MAPbI3 samples at 120°C.

# CHAPTER 4

# IMPROVED THERMAL STABILITY OF PEROVSKITE SOLAR CELLS WITH ADDED PMMA

The $Cs_xMA_{1-x}PbI_3$ films fabricated in this experiment follow the fabrication procedure as mentioned in Section 2.1 with the added PMMA layer. The $Cs_xMA_{1-x}PbI_3$ samples successfully showed stability over heating at extended period of hours (close to 1000 hours) for samples heated at 85°C. $Cs_xMA_{1-x}PbI_3$ samples heated at 120°C sustained a shorter period of stability due to the aggressiveness of the thermal treatment. This section will provide a detailed discussion and complete analysis of the data resulting from SEM, and XRD data.

## 4.1 $MAPbI_3$ with PMMA heated at 85℃

This section will discuss the $MAPbI_3$ sample fabricated with PMMA. The XRD peaks exist at 14.08°, and 28.44° corresponding to the perovskite (110), and (220) planes. In comparison to the XRD data presented in Figure 4, the $MAPbI_3$ peak in this data set shows a linear increase in perovskite height at (110). Even after 528 hours of thermal treatment, no $PbI_2$ peak was present at 12.6° as observed in Figure 11. Hence, the addition of PMMA aided in the passivation defects and prevented the sample from degrading upon exposure to the environmental degradation factors. As the sample is heated over time, the passivation of PMMA into the perovskite allows for the

$MAPbI_3$ sample to be less susceptible to degradation from heat. Therefore, it can be concluded that PMMA improved the thermal stability of the $MAPbI_3$ sample.

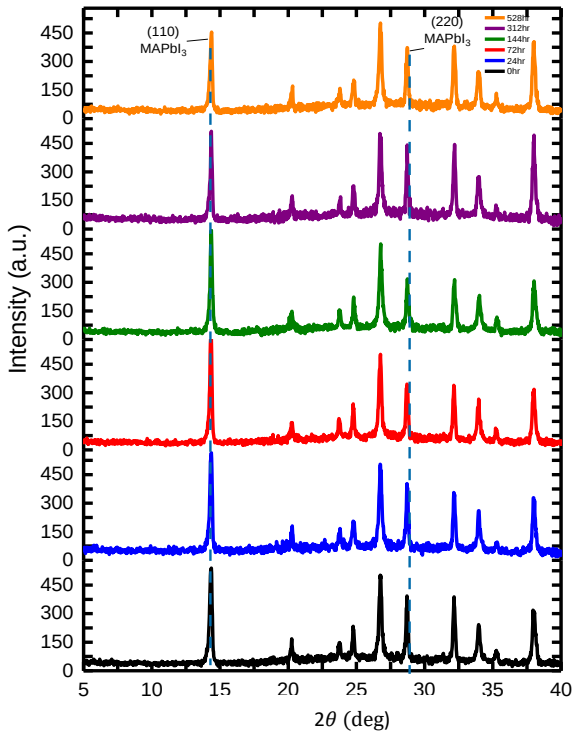


**Figure 11.** XRD data for the first 500 hours of measurement for $MAPbI_3$ with PMMA heated at 85°C.

The SEM images below show no indication of signs of degradation along the GBs and the grains. Figure 12shows a smooth surface with the "root-like" structure being somewhat centered along the grain. Upon heating for 72 hours, the "root-like" structure seems to be expanding towards the edge of the grains. It can be noted that in Figure 12(c) that the structure completely covers the grain, and formation of pinholes are starting to become more prominent along the edge of the grains. The SEM data shows how the structural stability of the sample reacts to the thermal treatment and provides a better insight about the morphological changes occurring. Although there

is formation of pinholes, no signs of degradation can be seen in the XRD data presented in Figure 11. This suggests that PMMA does change the morphological structure of the surface of the perovskite film, and passivate defective areas forming along the grain boundary of the sample.

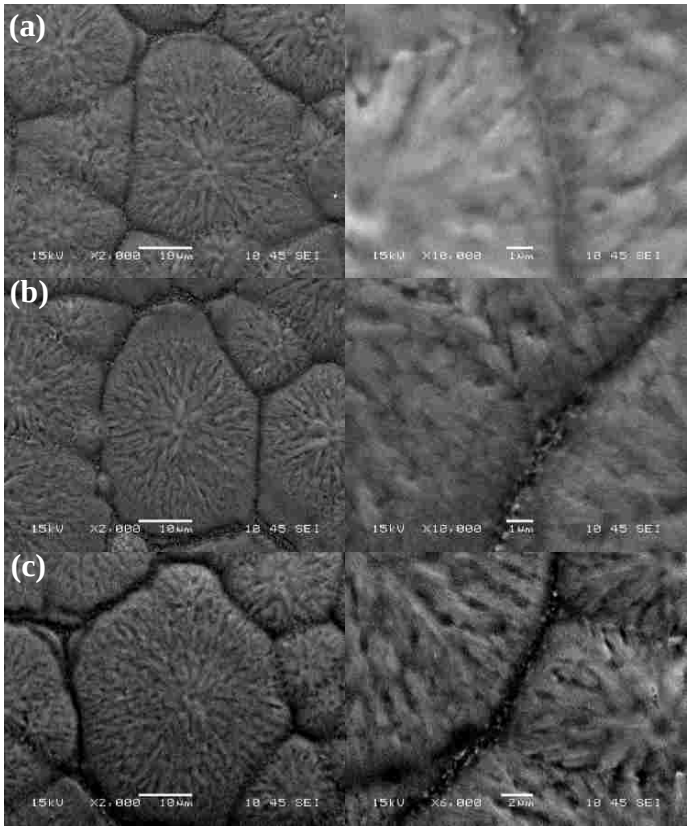


**Figure 12.** SEM image for MAPbI3 with PMMA heated at 85°C for (a) 0hr, (b) 72hr, and (c) 528hr.

Since the samples did not suffer or show any signs of degradation, the XRD integrated intensities plotted in Figure 13 correspond to the preferred orientation of $MAPbI_3$ peaks at (110) and (220). The integrated intensity for the (110) plane is much higher than that of the (220) plane, indicating that the $MAPbI_3$ sample fabricated preferred crystal growth along the (110) plane.

However, the two planes follow the same trend from which as the samples were heated over a period of 1000 hour.

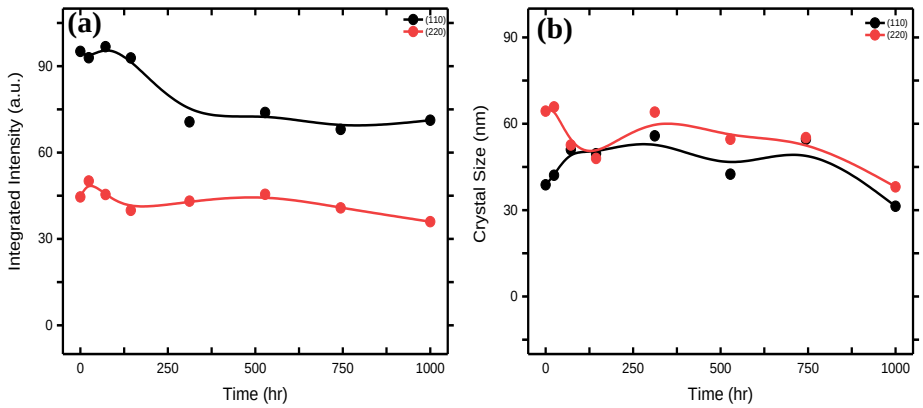


**Figure 13.** (a) XRD integrated intensity and (b) crystal size for planes (110) and (220) of $MAPbI_3$ with PMMA heated at 85°C.

Since the sample was able to withstand up to 528 hours of thermal treatment, it was furtherer treated to the standard thermal testing of 1000 hours. The XRD data indicates good thermal stability even until the 1000 hours thermal treatment. It is found that there is minor sign of the $PbI_2$ peak close to 1000 hours thermal heating, as shown in

Figure **14**(a). This could be a clear indication of an early sign of degradation, or it could also be due to the noise presented during the measurement. The SEM image below shows a smooth surface of the $MAPbI_3$ sample prior to thermal treatment. The “root-like” formation towards the center of the grain inhibits the same phenomenon as other samples upon thermal treatment, where the formation spreads to cover the entire grain. Prior to the thermal treatment, the SEM images showed no signs of degradation indicating a good film and morphological structure. Upon heating

for 528 hours, there are some signs of dark spots along the GBs, which could be pinholes forming. The XRD data, however, shows no indication of any signs of degradation or appearance of the $PbI_2$ peak. After 1000 hours of thermal treatment, the SEM images showed pinholes covering the very small grain sizes along the surface of the $MAPbI_3$ sample. The $10\mu m$ magnification indicates the complete degradation of smaller grains with several pinholes covering its surface. The larger grain sizes exhibit more pinholes forming along the GBs, but as indicated by the XRD data, there is minor sign of degradation. This could still be attributed to the effect of PMMA passivation on the surface morphology of the perovskite sample. As the samples are heated, the PMMA passivates onto the defective states and prevent any moisture and air from degrading the sample within. Thus, even with the morphological degradation occurring at the crystal grain of the $MAPbI_3$ sample, it remains stable with the help of PMMA.

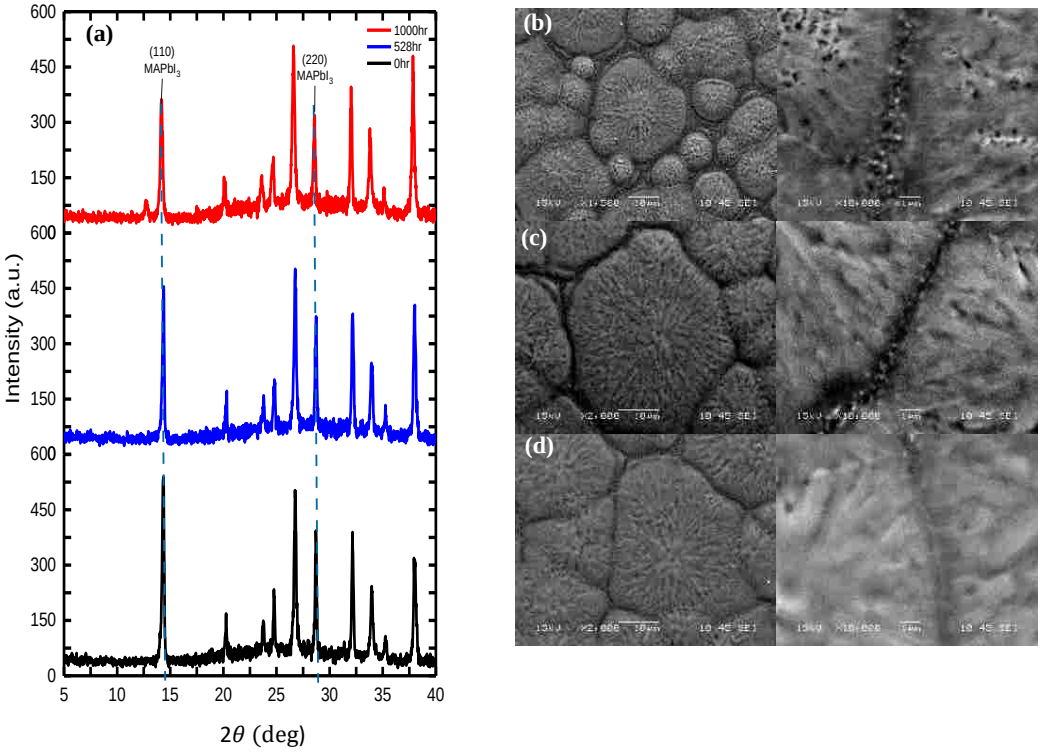

**Figure 14**. (a) XRD data and SEM images for (b) 1000hr, (c) 528hr, and (d) 0hr thermal treatment of $MAPbI_3$ with PMMA at 85°C.

### 4.2 $Cs_xMA_{1-x}PbI_3$ with PMMA heated at 85℃

This section will discuss the results for the $Cs_xMA_{1-x}PbI_3$ with PMMA thermally treated at 85℃. The XRD peaks exist at 14.08°, and 28.44° corresponding to the perovskite (110), and (220). The XRD data shows the decreasing peak of the $MAPbI_3$ height with increasing content of Cs as seen in

Figure **15** (a). Furthermore, the SEM images show that the "root-like" structure is more prominent for the x = 5% sample in comparison to the x = 20% sample as can be seen in

Figure **15**(d) and

Figure **15**(b), respectively. This "root-like" structure may be one of the main indication of the perovskite precursor solution and increasing the cesium content reduces this shape formation.

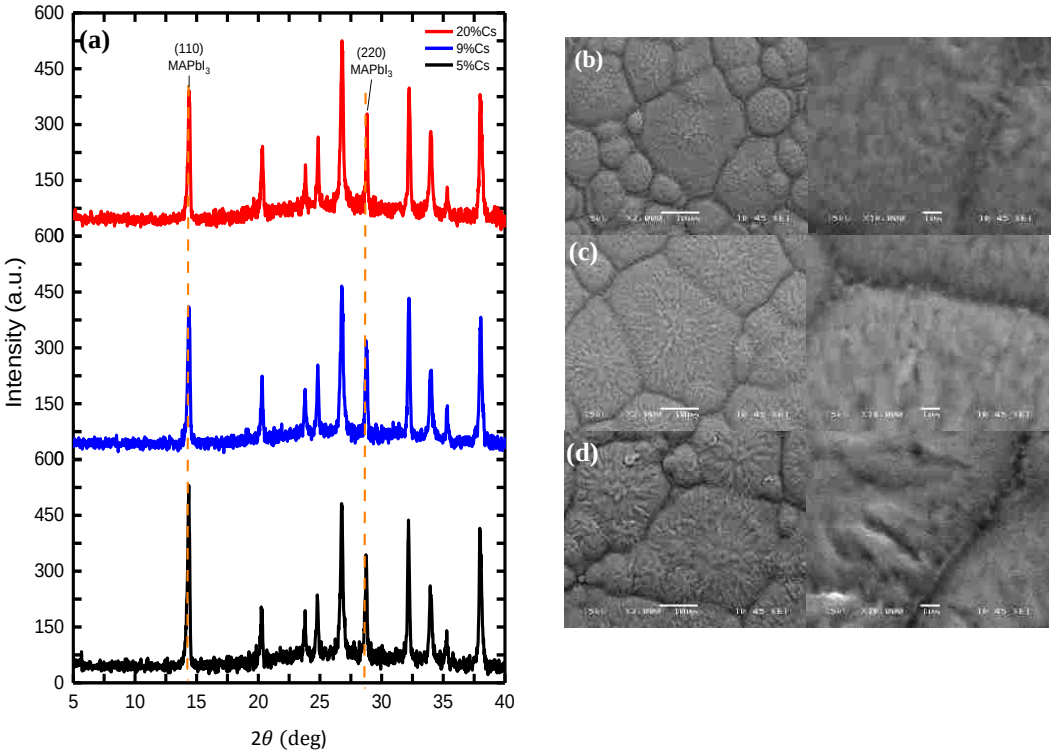


**Figure 15:** (a) XRD data and SEM images for (b) x = 20%, (c) x = 9%, and (d) x = 5% $Cs_xMA_{1-x}PbI_3$ with PMMA prior to thermal treatment.

After 500 hours of thermal heating, the $Cs_xMA_{1-x}PbI_3$ sample shows a slight decrease in the $MAPbI_3$ peak height for the x = 9% and x = 5% sample. However, the peak for the x = 20% sample increases slightly in comparison to the initial reading in

Figure **15**(a). From the SEM image in

Figure 16(b), the GBs along the small grains of the x = 20% sample is suffering from degradation. However, due to the addition of PMMA, these defects are passivated completely, given the slight increase in the perovskite peak at 14.08°. The film morphology for the x = 5% and

x = 9% prove to have a better film morphology than the sample with the x = 20% cesium content, as the grain structure for these samples are larger indicating less grain boundaries.

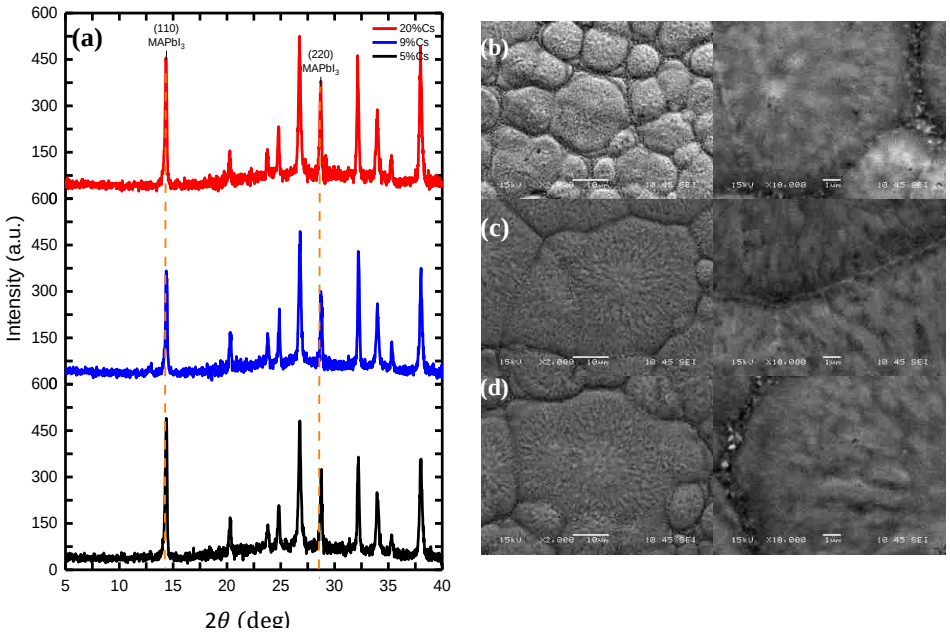


**Figure 16**. (a) XRD data and SEM images for (b) x = 20%, (c) x = 9%, and (d) x = 5% $Cs_xMA_{1-x}PbI_3$ with PMMA after 528 hours of thermal treatment.

The $Cs_xMA_{1-x}PbI_3$ were thermally treated to more than 1000 hours due to the stability of the previously studied $MAPbI_3$ sample, withstanding this amount of prolonged thermal treatment. **Error! Reference source not found.** shows the XRD data after 1000 hours of thermally heating the samples. It is clear to note that the $MAPbI_3$ height for the x = 20% sample had a 62% reduction. This sample initially had a lower poor film quality than the remaining samples, and therefore, confirming the higher percent increase in the perovskite peak. The remaining samples (x = 5% and x = 9%) saw a reduction in height but is not as significant as the reduction that the x = 20% sample presented after 1000 hours of thermal treatment. The appearance of the $PbI_2$ at 12.6° could have appeared due to scratches on the surface of the sample allowing for defective areas to penetrate

the perovskite crystal structure and cause degradation. This formation of peak could also be referred to as XRD noise by many, and not necessarily an indication of degradation. The $PbI_2$ peak height for the $Cs_xMA_{1-x}PbI_3$ is not as prominent as the $PbI_2$ peak in the samples without PMMA was mentioned in Chapter 3. This suggests that $Cs_xMA_{1-x}PbI_3$ with PMMA samples can withstand thermal treatment for prolonged periods of time (exceeding 1000 hours), so long as the samples are protected from scratches to prevent degradation from within.

**Figure 17.** (a) XRD data and SEM images for (b) x = 20%, (c) x = 9%, and (d) x = 5% CsxMA1-xPbI3 with PMMA after 1000 hours of thermal treatment.

### 4.3 $MAPbI_3$ with PMMA heated at 120℃

This section will discuss the $MAPbI_3$ samples with PMMA heated at 120℃. Samples were prepared as detailed win Section 2.1. The XRD peaks exist at 14.08°, and 28.44° corresponding to the perovskite planes at (110), and (220) and the $PbI_2$ peak at 12.6°, corresponding to the (001)

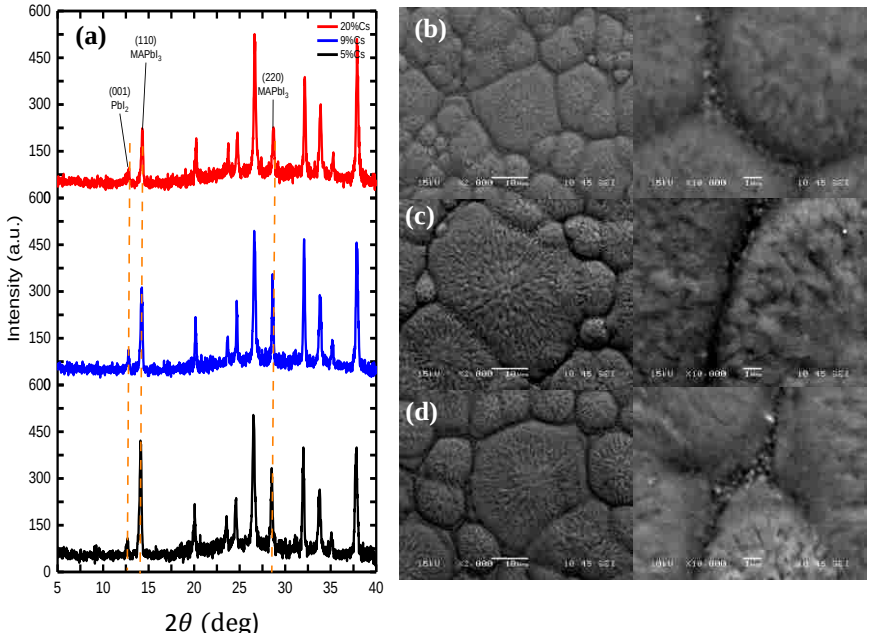


plane. As can be seen in

Figure **18.** XRD data for $MAPbI_3$ heated at 120℃ for 72 hours.

This was confirmed by the $PbI_2$ peak at 12.6° being four times the height of the perovskite peak at 14.08°. This data suggests the instability of MA-based perovskite solar cells at high temperatures, even with the additional help of passivated defects from PMMA. The captured SEM images in

Figure 19 show the increase of pinhole formation over the period of heating. The "root-like" structure mentioned previously, from which should relate to the perovskite decreases to a smaller diameter over time. This further confirms the degraded sample no longer have a high perovskite peak. , the $MAPbI_3$ sample exhibited complete degradation between the 24 and 72 hours reading. Upon taking the measurement at 72 hours, the $PbI_2$ peak height at 12.6° was already four times the height of the perovskite peak at 14.08°. Prior to degrading, the perovskite peak increased with the possibility of the PMMA passivating the defects and protecting the sample from degradation. Upon prolonged thermal treatment, the PMMA could no longer keep the sample stable due to the aggressiveness of the temperature heating

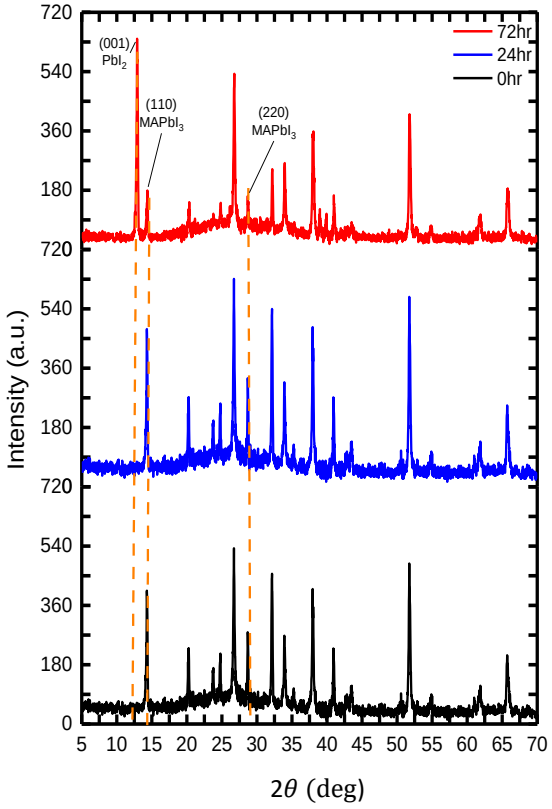


**Figure 18.** XRD data for $MAPbI_3$ heated at 120℃ for 72 hours.

This was confirmed by the $PbI_2$ peak at 12.6° being four times the height of the perovskite peak at 14.08°. This data suggests the instability of MA-based perovskite solar cells at high temperatures, even with the additional help of passivated defects from PMMA. The captured SEM images in

Figure 19 show the increase of pinhole formation over the period of heating. The "root-like" structure mentioned previously, from which should relate to the perovskite decreases to a smaller diameter over time. This further confirms the degraded sample no longer have a high perovskite peak.

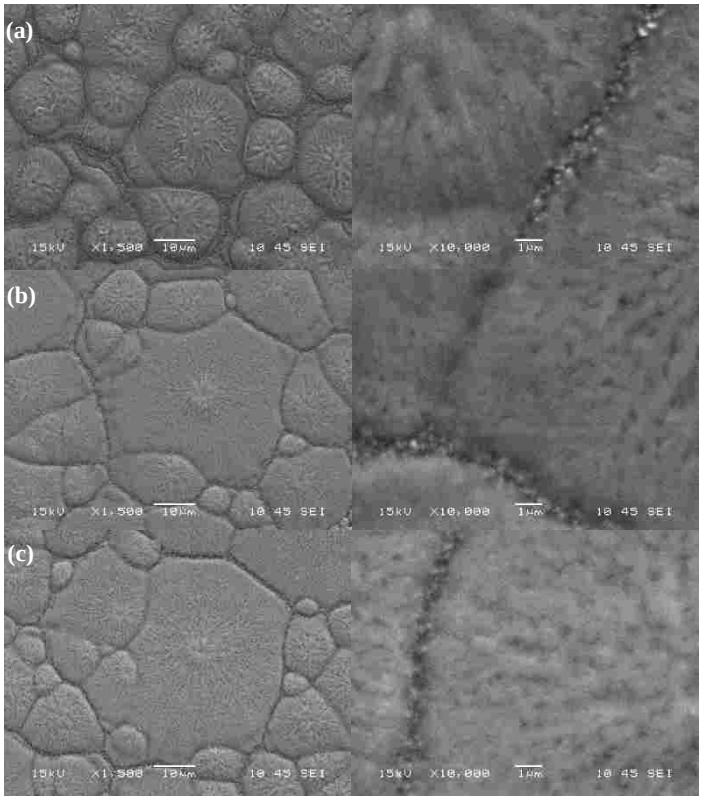


**Figure 19.** SEM images for $MAPbI_3$ thermally heated at 120°C for (a) 0hr, (b) 24hrs, and (c) 72hrs.

### 4.4 $Cs_xMA_{1-x}PbI_3$ with PMMA heated at 120℃

This section will discuss the results for the $Cs_xMA_{1-x}PbI_3$ with PMMA thermally heated at 120℃. The XRD peaks exist at 14.08°, and 28.44° corresponding to the perovskite planes at (110), and (220) and the $PbI_2$ peak at 12.6°, corresponding to the (001) plane. The samples in this section were induced to a higher heat temperature to observe whether PMMA and the additional Cs-doping will aid in the thermal stability of the perovskite solar cell. As Cs-based perovskites are known to withstand elevated temperatures reaching >300℃, we wanted to explore the effect of improving

the thermal stability of perovskite solar cells by doping the MA-based perovskites with cesium and adding PMMA to help passivate defects.

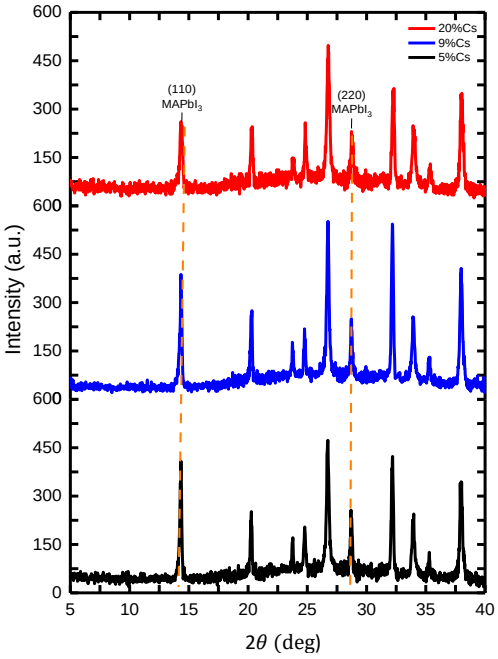


**Figure 20**. XRD data for $Cs_xMA_{1-x}PbI_3$ with PMMA prior to thermal treatment at 120°C.

$Cs_xMA_{1-x}PbI_3$ samples were only thermally treated for 72 hours upon discovery of the high $PbI_2$ peak at 12.6°. The prominence of the $PbI_2$ peak, however, is not that high in comparison to the $MAPbI_3$ sample mentioned in the previous section. Per the SEM image in

Figure 21. XRD data for $Cs_xMA_{1-x}PbI_3$ with PMMA thermally treated at 120°C for 72 hours(b), the x = 20% shows a relatively smooth feature with very few signs of pinholes. The x = 9% sample in

Figure 21. XRD data for $Cs_xMA_{1-x}PbI_3$ with PMMA thermally treated at 120°C for 72 hours(c), shows high prominence of pinholes along the GBs which led to the higher $PbI_2$ peak in the XRD data. The SEM image in

Figure 21. XRD data for $Cs_xMA_{1-x}PbI_3$ with PMMA thermally treated at 120°C for 72 hours(d) represents the x = 5%, showing signs of pinholes and scratches on the surface. However, even with these deformation and defects, the x = 5% sample was able to maintain similar peak heights for both the perovskite and $PbI_2$ peak. In comparison to the $MAPbI_3$ sample heated at the sample temperature with the same PMMA layer, this data shows clearly how the added cesium can aid in thermal stability of the sample. Comparing

Figure **18.** XRD data for $MAPbI_3$ heated at 120℃ for 72 hours.

This was confirmed by the $PbI_2$ peak at 12.6° being four times the height of the perovskite peak at 14.08°. This data suggests the instability of MA-based perovskite solar cells at high temperatures, even with the additional help of passivated defects from PMMA. The captured SEM images in

Figure 19 show the increase of pinhole formation over the period of heating. The “root-like” structure mentioned previously, from which should relate to the perovskite decreases to a smaller diameter over time. This further confirms the degraded sample no longer have a high perovskite peak. and

Figure 21. XRD data for $Cs_xMA_{1-x}PbI_3$ with PMMA thermally treated at 120°C for 72 hours, we see that the $PbI_2$ peak at the 72 hours reading for the $MAPbI_3$ sample is much higher than the $PbI_2$ peak for the Cs-doped samples. By doping perovskite samples with cesium, we see an improved thermal stability at elevated temperatures.

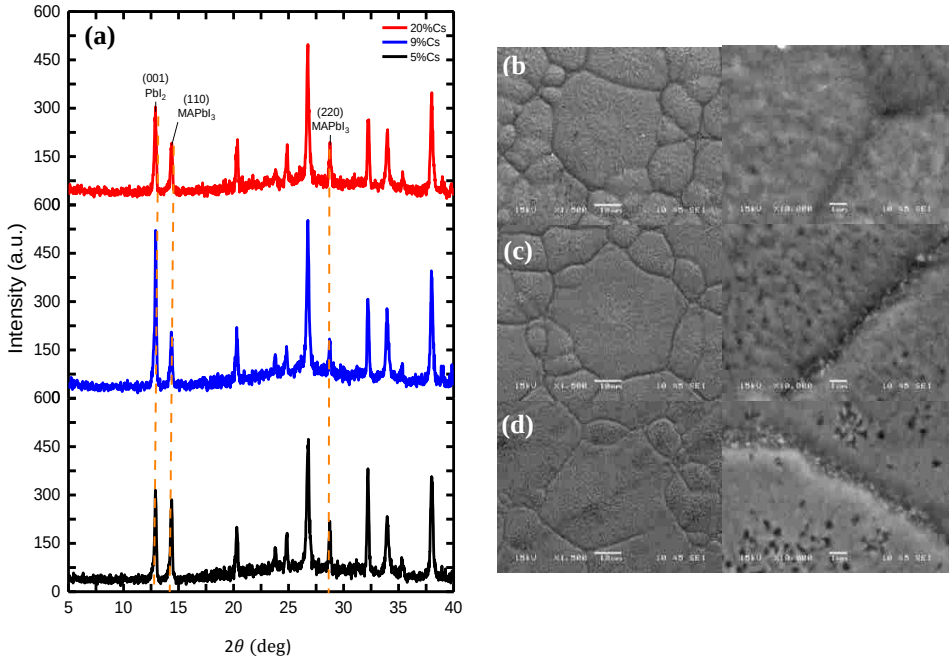


**Figure 21.** XRD data for $Cs_xMA_{1-x}PbI_3$ with PMMA thermally treated at 120°C for 72 hours.

# CHAPTER 5

# CONCLUSION

This thesis demonstrated the improved stability of $MAPbI_3$ and $Cs_xMA_{1-x}PbI_3$ perovskite solar cells with different concentrations of cesium (x = 5%, 9%, and 20%) with the added PMMA. Samples heated at 85°C without PMMA showed stability only until 72 hours before it started showing signs of degradation as seen in the XRD data and SEM images. Furthermore, $MAPbI_3$ and $Cs_xMA_{1-x}PbI_3$ heated at 85°C degraded completely after 500 hours of thermal heating. In comparison, samples with the added PMMA layer were able to withstand prolonged heating up to 1000 hours. The added PMMA layer aided in passivating the defective areas along the grain boundaries and protected the device from degradation due to heat. To further confirm the improved stability of perovskite solar cells with PMMA, samples were induced to heating at 120°C. Herein, we observed that the samples degraded between at the 72 hours heating. The $MAPbI_3$ sample showed the highest degradation rate in comparison to the samples with the cesium content. Because of the aggressive of the temperature, PMMA was not able to keep the sample thermally stable for longer periods of time. However, the Cs-doped perovskite samples were able to show good stability with the XRD data showing that the height difference between the perovskite peak and the $PbI_2$ peak is not that high in comparison to the $MAPbI_3$ samples. Therefore, it is clear to say that PMMA aided in the passivation of defects and improving the stability of perovskite solar cells at lower temperatures. Addition of Cs is needed, however, to further improve the thermal stability of perovskite solar cells at higher temperatures.

## REFERENCES

[1] B. Sørensen, "A history of renewable energy technology", *Energy Policy*, vol. 19, no. 1, pp. 8-12, 1991.

[2] "Fossil Fuels", *Eesi.org*, 2018. [Online]. Available: http://www.eesi.org/topics/fossil-fuels/description. [Accessed: 29- Mar- 2018].

[3] International Energy Agency (IEA), "Key World Energy Statistics 2017", IEA, 2017.

[4] International Energy Agency (IEA), "World Energy Outlook 2017", IEA, 2017.

[5] "Solar Explained: Photovoltaic and Electricity", *Eia.gov*, 2017. [Online]. Available: https://www.eia.gov/energyexplained/index.cfm?page=solar_photovoltaics. [Accessed: 29- Mar- 2018].

[6] M. Lee, J. Teuscher, T. Miyasaka, T. Murakami and H. Snaith, "Efficient Hybrid Solar Cells Based on Meso-Superstructured Organometal Halide Perovskites", *Science*, vol. 338, no. 6107, pp. 643-647, 2012.

[7] J. Burschka, N. Pellet, S. Moon, R. Humphry-Baker, P. Gao, M. Nazeeruddin and M. Grätzel, "Sequential deposition as a route to high-performance perovskite-sensitized solar cells", *Nature*, vol. 499, no. 7458, pp. 316-319, 2013.

[8] H. Zhou, Q. Chen, G. Li, S. Luo, T. Song, H. Duan, Z. Hong, J. You, Y. Liu and Y. Yang, "Interface engineering of highly efficient perovskite solar cells", *Science*, vol. 345, no. 6196, pp. 542-546, 2014.

[9] N. Park, "Perovskite solar cells: an emerging photovoltaic technology", *Materials Today*, vol. 18, no. 2, pp. 65-72, 2015.

[10] J. Lee, D. Kim, H. Kim, S. Seo, S. Cho and N. Park, "Formamidinium and Cesium Hybridization for Photo- and Moisture-Stable Perovskite Solar Cell", *Advanced Energy Materials*, vol. 5, no. 20, p. 1501310, 2015.

[11] G. Eperon, S. Stranks, C. Menelaou, M. Johnston, L. Herz and H. Snaith, "Formamidinium lead trihalide: a broadly tunable perovskite for efficient planar heterojunction solar cells", *Energy & Environmental Science*, vol. 7, no. 3, p. 982, 2014.

[12] H. Tang, S. He and C. Peng, "A Short Progress Report on High-Efficiency Perovskite Solar Cells", *Nanoscale Research Letters*, vol. 12, no. 1, 2017.

[13] T. Leijtens, K. Bush, R. Cheacharoen, R. Beal, A. Bowring and M. McGehee, "Towards enabling stable lead halide perovskite solar cells; interplay between structural, environmental, and thermal stability", *Journal of Materials Chemistry A*, vol. 5, no. 23, pp. 11483-11500, 2017.

[14] P. Whitfield, N. Herron, W. Guise, K. Page, Y. Cheng, I. Milas and M. Crawford, "Structures, Phase Transitions and Tricritical Behavior of the Hybrid Perovskite Methyl Ammonium Lead Iodide", *Scientific Reports*, vol. 6, no. 1, 2016.

[15] R. Ginting, M. Jeon, K. Lee, W. Jin, T. Kim and J. Kang, "Degradation mechanism of planar-perovskite solar cells: correlating evolution of iodine distribution and photocurrent hysteresis", *Journal of Materials Chemistry A*, vol. 5, no. 9, pp. 4527-4534, 2017.

[16] Z. Fan, H. Xiao, Y. Wang, Z. Zhao, Z. Lin, H. Cheng, S. Lee, G. Wang, Z. Feng, W. Goddard, Y. Huang and X. Duan, "Layer-by-Layer Degradation of Methylammonium Lead Tri-iodide Perovskite Microplates", *Joule*, vol. 1, no. 3, pp. 548-562, 2017.

[17] B. Li, Y. Li, C. Zheng, D. Gao and W. Huang, "Advancements in the stability of perovskite solar cells: degradation mechanisms and improvement approaches", *RSC Advances*, vol. 6, no. 44, pp. 38079-38091, 2016.

[18] Q. Dao, R. Tsuji, A. Fujii and M. Ozaki, "Study on degradation mechanism of perovskite solar cell and their recovering effects by introducing CH3NH3I layers", 2018.

[19] B. Sutherland, "Thermally Decomposing Perovskites One Layer at a Time", Joule, vol. 1, no. 3, pp. 423-424, 2017.

[20] M. Green, K. Emery, K. Bücher, D. King and S. Igari, "Solar cell efficiency tables (version 10)", *Progress in Photovoltaics: Research and Applications*, vol. 5, no. 4, pp. 265-268, 1997.

[21] M. Green, Y. Hishikawa, E. Dunlop, D. Levi, J. Hohl-Ebinger and A. Ho-Baillie, "Solar cell efficiency tables (version 51)", *Progress in Photovoltaics: Research and Applications*, vol. 26, no. 1, pp. 3-12, 2017.

[22] A. Louwen, W. van Sark, R. Schropp and A. Faaij, "A cost roadmap for silicon heterojunction solar cells", *Solar Energy Materials and Solar Cells*, vol. 147, pp. 295-314, 2016.

[23] W. Kong, T. Ding, G. Bi and H. Wu, "Optical characterizations of the surface states in hybrid lead–halide perovskites", *Physical Chemistry Chemical Physics*, vol. 18, no. 18, pp. 12626-12632, 2016

[24] F. Wang, A. Shimazaki, F. Yang, K. Kanahashi, K. Matsuki, Y. Miyauchi, T. Takenobu, A. Wakamiya, Y. Murata and K. Matsuda, "Highly Efficient and Stable Perovskite Solar Cells by Interfacial Engineering Using Solution-Processed Polymer Layer", The Journal of Physical Chemistry C, vol. 121, no. 3, pp. 1562-1568, 2017.

[25] C. Awino, V. Odari and T. Sakwa, "Investigation of Structural and Electronic Properties of CH3NH3PbI3 Stabilized by Varying Concentrations of Poly(Methyl Methacrylate) (PMMA)", Coatings, vol. 7, no. 8, p. 115, 2017.

[26] M. Taguchi, A. Suzuki, H. Tanaka and T. Oku, "Fabrication and characterization of perovskite solar cells added with MnCl2, YCl3 or poly(methyl methacrylate)", 2018.

[27] L. Ono, N. Park, K. Zhu, W. Huang and Y. Qi, "Perovskite Solar Cells—Towards Commercialization", *ACS Energy Letters*, vol. 2, no. 8, pp. 1749-1751, 2017.

[28] G. Niu, W. Li, J. Li, X. Liang and L. Wang, "Enhancement of thermal stability for perovskite solar cells through cesium doping", *RSC Advances*, vol. 7, no. 28, pp. 17473-17479, 2017.

[29] P. Fan, D. Gu, G. Liang, J. Luo, J. Chen, Z. Zheng and D. Zhang, "High-performance perovskite CH3NH3PbI3 thin films for solar cells prepared by single-source physical vapour deposition", *Scientific Reports*, vol. 6, no. 1, 2016.

[30] S. Raga, M. Jung, M. Lee, M. Leyden, Y. Kato and Y. Qi, "Influence of Air Annealing on High Efficiency Planar Structure Perovskite Solar Cells", *Chemistry of Materials*, vol. 27, no. 5, pp. 1597-1603, 2015.

[31] N. Kim, Y. Min, S. Noh, E. Cho, G. Jeong, M. Joo, S. Ahn, J. Lee, S. Kim, K. Ihm, H. Ahn, Y. Kang, H. Lee and D. Kim, "Investigation of Thermally Induced Degradation in CH3NH3PbI3 Perovskite Solar Cells using In-situ Synchrotron Radiation Analysis", Scientific Reports, vol. 7, no. 1, 2017.

[32] E. Juarez-Perez, Z. Hawash, S. Raga, L. Ono and Y. Qi, "Thermal degradation of CH3NH3PbI3 perovskite into NH3 and CH3I gases observed by coupled thermogravimetry–mass spectrometry analysis", Energy & Environmental Science, vol. 9, no. 11, pp. 3406-3410, 2016.

[33] Q. Dao, R. Tsuji, A. Fujii and M. Ozaki, "Study on degradation mechanism of perovskite solar cell and their recovering effects by introducing CH3NH3I layers", *Organic Electronics*, vol. 43, pp. 229-234, 2017.

[34] B. Dutrow and C. Clark, "X-ray Powder Diffraction (XRD)", *Integrating Research and Education*. [Online]. Available: https://serc.carleton.edu/research_education/geochemsheets/techniques/XRD.html. [Accessed: 25- Feb- 2018].

[35] "Characteristic X-Rays", *HyperPhysics*. [Online]. Available: http://hyperphysics.phy-astr.gsu.edu/hbase/quantum/xrayc.html. [Accessed: 25- Feb- 2018].

[36] J. Jordan, "What is x-ray diffraction?", *Jeremy's Blog*, 2016. [Online]. Available: https://www.jeremyjordan.me/what-is-x-ray-diffraction/. [Accessed: 25- Feb- 2018].

**VITA**

Christine M. Gausin
Department of Electrical and Computer Engineering
Old Dominion University
Norfolk, VA 23529

## EDUCATION

Old Dominion University
B.S in Electrical Engineering 2017

## HONORS, AWARDS, Scholarships

- SoLar Engineering Academic Program (SoLEAP) Scholarship, National Science Foundation, Award # 1355678, 2016 – 2018

## RELATED EXPERIENCE

- Student Trainee – Naval Surface Warfare Center Dahlgren Division Dam Neck Activity (DNA), Dam Neck, VA
  August 2017 – Present
- Student Trainee – Naval Surface Warfare Center Dahlgren Division, Dahlgren, VA
  May 2014 – August 2017